Available online at www.sciencedirect.com
ScienceDirect
International Journal of Heat and Mass Transfer 50 (2007) 2828–2837
International Journal of HEAT and MASS TRANSFER
www.elsevier.com/locate/ijhmt

Inverse radiation–conduction design problem in a participating concentric cylindrical medium

Ki Wan Kim *, Seung Wook Baek

Division of Aerospace Engineering, Department of Mechanical Engineering, Korea Advanced Institute of Science and Technology, 373-1, Guseong-Dong, Yuseong-Gu, Daejeon 305-701, Republic of Korea

Received 10 January 2006; received in revised form 23 October 2006
Available online 13 March 2007

Abstract

Inverse conduction–radiation problem for design analysis in a two-dimensional concentric cylindrical absorbing, emitting and isotropically scattering medium has been solved, when the desired boundary conditions are available on the design surface. The finite-volume method was adopted to deal with energy conservation equation including conduction and radiation. The radiative transfer equation was also taken into consideration in direct problem, whereas the Levenberg–Marquardt method was used to solve a set of equations in inverse problem, which are expressed by errors between estimated and desired total heat fluxes on the design surface. The automatic differentiation as well as the Broyden combined update was utilized to reduce computational time in calculating the sensitivity matrix. The results have shown that the desired total heat flux distribution on design surface could be successfully estimated with less computational time using the present inverse procedure developed here.

Keywords: Inverse radiation–conduction problem; Automatic differentiation; Broyden combined update; Levenberg–Marquardt Method; Concentric cylindrical medium

1. Introduction

Heat transfer by conduction and radiation is an important combined heat transfer mode in various engineering design problems such as fibrous insulation and glass manufacturing industry. Consequently, the combined conduction and radiation, especially, in cylindrical geometry has been studied by many researchers [1–3]. In these reference, the total heat flux on a side wall or temperature field was calculated when boundary conditions were given.

Recently, inverse heat transfer analysis has received much attention due to its various applications [4]. Among others, especially, the inverse conduction–radiation analysis was applied to estimate the thermal properties or to deduce the optimal condition that satisfies a design goal. In the former case, Matthews et al. estimated the extinction coefficient, back scattering fraction, and thermal conductivity when the temperature and transmittance measurements are given in one-dimensional planar layer [5]. Ruperti et al. predicted the surface temperature and heat fluxes from simulated transient temperature data in one-dimensional semi-transparent slab [6]. Li simultaneously estimated the single scattering albedo, the optical thickness, the conduction-to-radiation parameter, and the scattering phase function with the exit radiation intensities in a one-dimensional plane-parallel medium using the conjugate gradient method in parameter estimation approach [7]. In the latter case, a boundary design problem was solved to obtain optimal distribution of the heater powers located on the heater surface which satisfies a desired heat flux distribution on design surface in two-dimensional irregular domain using the conjugate gradient method [8]. However, such a problem has not been explored in a cylindrical geometry so far.

A successful estimation of unknown properties depends on the magnitude of sensitivity coefficient. The bigger its

* Corresponding author. Tel.: +82 42 869 3754; fax: +82 42 869 3710.
E-mail address: kiwankim@kaist.ac.kr (K.W. Kim).

0017-9310/$ - see front matter © 2007 Elsevier Ltd. All rights reserved.
doi:10.1016/j.ijheatmasstransfer.2006.10.056

Nomenclature

D_{ci}	direction weights
E_b	emissive power, σT^4, W/m^2
$\vec{e}_x, \vec{e}_y, \vec{e}_z$	unit vector in x, y, z directions
G	incident radiation
I	radiation intensity, W/(m^2 sr)
I_b	blackbody radiation intensity, W/(m^2 sr)
k	thermal conductivity, W/m K
L	cylinder height, m
$\vec{n}_i$	unit vector normal to control volume surface i
N_{CR}	conduction-to-radiation parameter ($= k\beta/4\sigma T_{ref}^3$)
n_c	number of code events
n_e	number of elements on design surface
n_p	number of unknown parameters
$\mathbf{P}$	vector of unknown parameters
q_C	conductive heat flux, W/m^2
q_R	radiative heat flux, W/m^2
q_T	total heat flux, W/m^2
r	radial coordinate
$\vec{r}$	position vector of intensity
r_{in}	inner cylinder radius, m
r_{out}	outer cylinder radius, m
$\mathbf{S}$	equations set
$\hat{s}$	direction vector of intensity
T	temperature of participating medium, K
T_i	boundary temperature at the surface i
$\mathbf{X}$	sensitivity matrix
z	axial coordinate

Greeks symbols

β_0	extinction coefficient, $\kappa_a + \sigma_s$, m^{-1}
$\Delta A_i, \Delta V$	ith surface area and volume of the control volume
$\Delta\Omega$	control angle
ε_i	boundary emissivity at the surface i
Φ	scattering phase function
φ_0	space variable in the azimuthal direction measured from x-axis, rad
φ_Ω	angular variable in the azimuthal direction measured from x'-axis, rad
κ_a	absorption coefficient, m^{-1}
μ	damping parameter
θ	polar angle measured from the z-direction, rad
Θ	non-dimensional medium temperature
σ	Stefan–Boltzmann constant, 5.67×10^{-8} W/m^2 K^4
σ_s	scattering coefficient, m^{-1}
τ	optical thickness
$\mathbf{\Omega}$	diagonal matrix
ω_0	single scattering albedo

Subscripts

C	conduction
d	design surface
E, W, N, S, T, B	index of neighboring nodal points
e, w, n, s, t, b	index of control volume surfaces
e	estimated value
h	heater surface
P	calculating nodal point
R	radiation
ref	reference value
T	conduction + radiation
w	wall

Superscripts

m, m'	radiation direction
m^+, m^-	boundaries of the control volume
k	iteration number
$*$	non-dimensional quantity
0	initial value

magnitude, the easier it is to estimate the relevant inverse solutions. Furthermore, a reduction in computational time for calculating those values is one of main issues in using the gradient-based inverse method. Sensitivity method is necessary to approximate sensitivity coefficients. So far, the equation-based sensitivity methods, such as sensitivity problem [4], boundary value problem [4,8] or adjoint problem [4], have been prevalent. The finite-difference approximation was also used to calculate the sensitivity matrix [7]. Recently, the code-based method has received much attention due to its own advantage [9], since it does not need to derive an adjoint problem or sensitivity problem, which is required in gradient-based method, so that a discretization procedure of relevant equations is not necessary. In using the code-based method the computational code for calculating sensitivity matrix can be directly extracted from the code of direct problem. The automatic differentiation belongs to this category [10].

In this paper, inverse conduction–radiation design analysis in a two-dimensional concentric cylindrical absorbing, emitting and scattering medium has been conducted, given desired boundary conditions on the design surface. Finite-volume method was adopted to deal with the energy conservation equation and the radiative transfer equation in direct problem, whereas the Levenberg–Marquardt method was used as the inverse method. The Broyden combined update, which is one of the secant methods, was used with automatic differentiation to further shorten the computational time required to calculate the sensitivity matrix. In inverse analysis, a parametric analysis was conducted to examine the effects of boundary temperature, surface emissivity, a ratio of cylinder length to outer radius, and

conduction-to-radiation parameter on total heat flux distribution on heater surface. Inverse method was also applied to a real design problem to get the total heat flux on heater surface satisfying uniform total heat flux and temperature distribution on design surface.

Therefore, the major objective of this work is to propose the automatic differentiation combined with the Broyden combined update as an alternative sensitivity method and to extend the inverse conduction–radiation design problem to a two-dimensional cylindrical enclosure as its practical application.

2. Analysis and modeling

2.1. Model description

Fig. 1 shows a concentric cylindrical enclosure which is filled with an absorbing, emitting, and scattering gray medium, and its simplified geometry with boundary conditions. The walls are diffusely emitting and reflecting gray walls.

The direct problem is to calculate the total heat flux distribution on design surface 1, given the boundary conditions such as temperature, wall emissivity, and the medium properties such as single scattering albedo, extinction coefficient and conduction-to-radiation parameter. Temperature distribution inside the medium is determined by solving the energy conservation equation. Radiative heat flux on the wall including heater surface 2 and design surface 1 is obtained by integrating the dot product of intensity and unit normal vector over all solid angles, while

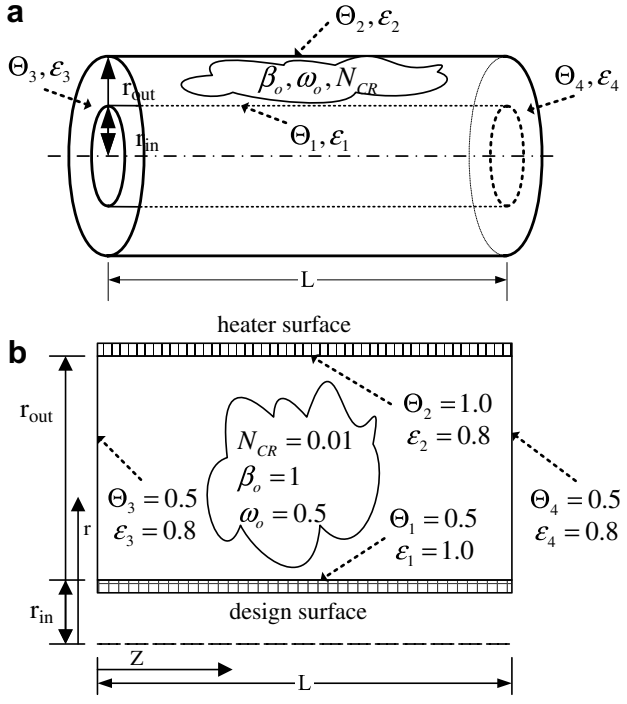

Fig. 1. Schematic of the physical system and its simplified geometry: (a) physical system and (b) simplified geometry ($L = 4$, $r_{out} = 1$, $r_{in} = 0.5$).

intensity distribution is acquired by solving the radiative transfer equation. In this work, the finite-volume method is adopted for solving the radiative transfer equation and energy conservation equation.

In inverse problem, the goal is to find the total heat flux distribution on heater surface 2 which satisfies the desired total heat flux as well as temperature on design surface 1. The Levenberg–Marquardt method is used to solve a set of equations expressed by errors between estimated and desired total heat flux on design surface. In order to diminish computing time for calculating sensitivity matrix, a combined method of automatic differentiation and Broyden combined update is adopted in this study.

Detailed description of mathematical formulations and numerical methods used in this work is given below.

2.2. Governing equation

Non-dimensional energy conservation equation governing the steady-state combined conduction and radiation heat transfer is defined by

$$\nabla^2\Theta - \frac{(1-\omega_o)}{N_{\mathrm{CR}}}(G^* - \Theta^4) = 0 \tag{1}$$

where $\Theta = \frac{T}{T_{\mathrm{ref}}}, \omega_0 = \frac{\sigma_s}{\beta_o}, N_{\mathrm{CR}} = \frac{k\beta}{4\sigma T_{\mathrm{ref}}^3}$ and $\beta_0 = \kappa_a + \sigma_s$. Here, all thermal properties are assumed constant, while $G^* = \frac{G}{4E_b} = \frac{1}{4\pi}\int_{4\pi} I^*(\vec{r}, \hat{s})\,\mathrm{d}\Omega$ is the dimensionless incident radiation obtained by solving the radiative transfer equation.

Non-dimensionalized radiative transfer equation governing the radiation intensity for a gray medium at any position $\vec{r}$ along a path $\hat{s}$ through an absorbing, emitting, and isotropically scattering medium is given by

$$\frac{\mathrm{d}I^*(\vec{r}, \hat{s})}{\mathrm{d}\tau} + I^*(\vec{r}, \hat{s}) = (1-\omega_o)\Theta^4 + \frac{\omega_o}{4\pi}\int_{4\pi} I^*(\vec{r}, \hat{s})\,\mathrm{d}\Omega' \tag{2}$$

where $I^* = \frac{I}{I_b(T_{\mathrm{ref}})}$ and $\tau = \beta_o s$.

The boundary condition for a diffusely emitting and reflecting wall can be written as follows:

$$I^*(\vec{r}_w, \hat{s}) = \varepsilon_w(\vec{r}_w)\Theta^4(\vec{r}_w) + \frac{1-\varepsilon_w(\vec{r}_w)}{\pi} \times \int_{\hat{s}'\cdot\vec{n}_w<0} I^*(\vec{r}_w, \hat{s}')|\,\hat{s}'\cdot\vec{n}_w|\,\mathrm{d}\Omega' \tag{3}$$

where ε_w is the wall emissivity and $\vec{n}_w$, which has a positive value when the ray travels from the wall to medium, is the unit normal vector to the wall. The finite-volume method was adopted to obtain the discretizatized equation of energy conservation equation, Eq. (1) [11].

The dimensionless radiative and conductive heat fluxes are calculated as follows:

$$q_R^*(\vec{r}_w) = \frac{q_R}{4E_b} = \frac{1}{4\pi}\int_{4\pi} I^*(\vec{r}_w, \hat{s})(\vec{n}_w \cdot \hat{s})\,\mathrm{d}\Omega \tag{4}$$

$$q_C^*(\vec{r}_w) = \frac{q_C}{4E_b} = -N_{\mathrm{CR}}\nabla\Theta \tag{5}$$

Finally, the dimensionless total heat flux is given by

$$q_{\mathrm{T}}^{*}(\vec{r}_{\mathrm{w}}) = q_{\mathrm{C}}^{*}(\vec{r}_{\mathrm{w}}) + q_{\mathrm{R}}^{*}(\vec{r}_{\mathrm{w}}). \tag{6}$$

In this study, the downward direction is defined as positive for the total heat flux on design and heater surface.

2.3. Finite-volume method (FVM) for radiation

In solving the radiative transfer equation, the FVM is adopted for its convenience in selecting the solid angle while guaranteeing an exact global conservation of radiative energy. The Chui's way to treat the axisymmetric geometry is employed here [12]. To obtain the discretized form of equation, Eq. (2) is integrated over a control volume, ΔV, and a control angle, $\Delta\Omega^m$, in the axisymmetric orthogonal grid as shown in Fig. 2. By assuming that the magnitude of the intensity in a control volume and control angle is constant, the following finite-volume formulation can be obtained:

$$\sum_{i=e,w,n,s,t,b} I_i^{*,m}\Delta A_i D_{ci}^m = (-I_P^{*,m} + S_{r,P}^{*,m})\Delta V\Delta\Omega^m \tag{7a}$$

where

$$D_{ci}^m = \int_{\varphi_\Omega^{m-}}^{\varphi_\Omega^{m+}}\int_{\theta^{m-}}^{\theta^{m+}} (\hat{s}\cdot\vec{n}_i)\sin\theta\,\mathrm{d}\theta\,\mathrm{d}\varphi_\Omega \tag{7b}$$

$$\hat{s} = \sin\theta\cos\varphi_\Omega\vec{e}_x + \sin\theta\sin\varphi_\Omega\vec{e}_y + \cos\theta\vec{e}_z \tag{7c}$$

$$\vec{n}_e = \sin\varphi_{0,P-}\vec{e}_x - \cos\varphi_{0,P-}\vec{e}_y \tag{7d}$$

$$\vec{n}_{\mathrm{w}} = -\sin\varphi_{0,P+}\vec{e}_x + \cos\varphi_{0,P+}\vec{e}_y \tag{7e}$$

$$\vec{n}_n = -\vec{n}_s = \cos\varphi_{o,P}\vec{e}_x + \sin\varphi_{o,P}\vec{e}_y \tag{7f}$$

$$\vec{n}_t = -\vec{n}_b = \vec{e}_z \tag{7g}$$

$$S_r^{*,m} = (1-\omega_0)\Theta^4 + \frac{\omega_0}{4\pi}\int_{\Omega'=4\pi} I^{*,m'}\Phi_{m'\to m}\,\mathrm{d}\Omega' \tag{7h}$$

$$\Delta\Omega^m = \int_{\varphi_\Omega^{m-}}^{\varphi_\Omega^{m+}}\int_{\theta^{m-}}^{\theta^{m+}} \sin\theta\,\mathrm{d}\theta\,\mathrm{d}\varphi_\Omega \tag{7i}$$

In order to relate the intensities on the control volume surfaces to the nodal one, the step scheme, which is not only simple and convenient, but also ensures positive intensity, is adopted. Then, the final discretized equation for FVM becomes

$$a_P^m I_P^{*,m} = \sum_{I=E,W,S,N,T,B} a_I^m I_I^{*,m} + b_P^m \tag{8a}$$

$$a_I^m = -\Delta A_i D_{ci,\mathrm{in}}^m \tag{8b}$$

$$a_P^m = \sum_{i=e,w,s,n,t,b} \Delta A_i D_{ci,\mathrm{out}}^m + \Delta V\Delta\Omega^m \tag{8c}$$

$$b_P^m = (S_{r,P}^{*,m})\Delta V\Delta\Omega^m \tag{8d}$$

where

$$D_{ci,\mathrm{out}}^m = \int_{\Delta\Omega^m} (\vec{n}_i\cdot\hat{s})\mathrm{d}\Omega\,\vec{n}_i\cdot\hat{s} > 0 \tag{8e}$$

$$D_{ci,\mathrm{in}}^m = \int_{\Delta\Omega^m} (\vec{n}_i\cdot\hat{s})\mathrm{d}\Omega\,\vec{n}_i\cdot\hat{s} < 0 \tag{8f}$$

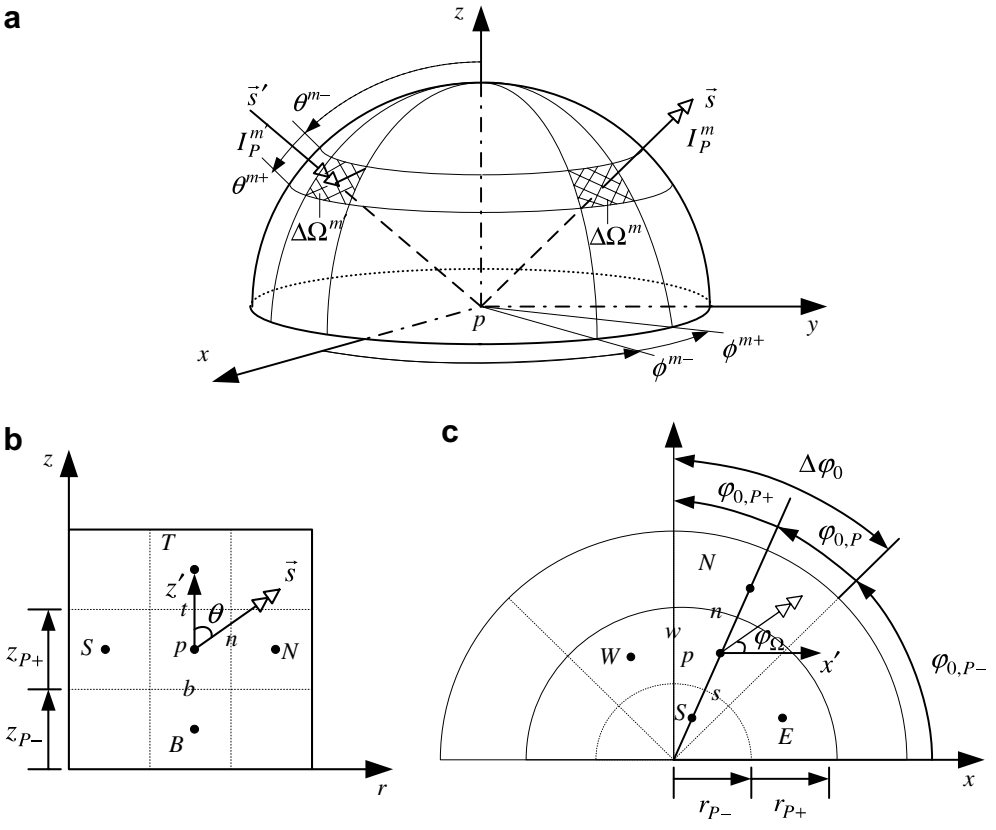

Fig. 2. Angular control angle and spatial control volume: (a) angular control angle and (b) spatial control volume.

The spatial and angular domains are discretized into 50×50 control volumes and 8×20 control angles.

2.4. Levenberg–Marquardt method (LMM)

In applying the quasi–Newton's method to inverse analysis, a set of equations has to be formulated using the difference between the estimated and desired heat flux on design surface as follows:

$$S_i(\mathbf{P}) = q^*_{T,e,i}(\mathbf{P}) - q^*_{T,d,i} \quad \text{for } i = 1, \ldots, n_e \tag{9}$$

Here, $\mathbf{P}$ is unknown parameter, which is a temperature distribution required on heater surface, Θ_2, in this work. In the above equation, $\mathbf{S}$ can be expressed in Taylor series, and should converge to zero while finding appropriate parameters such that

$$\mathbf{S}(\mathbf{P}) \cong \mathbf{S}^0(\mathbf{P}^0) + \nabla\mathbf{S}(\mathbf{P})(\mathbf{P} - \mathbf{P}^0) = 0 \tag{10}$$

where $\nabla\mathbf{S}(\mathbf{P}) = \frac{\partial \mathbf{S}(\mathbf{P})}{\partial \mathbf{P}} = \frac{\partial q^*_{T,e}(\mathbf{P})}{\partial \mathbf{P}}$, which is the matrix of sensitivity coefficients, $\mathbf{X}$.

After some manipulation of Eq. (10), we can derive the following relation:

$$\mathbf{P}^{k+1} = \mathbf{P}^k - (\mathbf{X}^k)^{-1}\mathbf{S}^k \tag{11}$$

Here, it must be noted that the above relation may be applied only for the case that the number of equations is the same as that of unknown variables. However, based on the fact that the number of equations can be greater than that of unknown variables in the inverse analysis, Eq. (11) is modified as follows:

$$\mathbf{P}^{k+1} = \mathbf{P}^k - [(\mathbf{X}^k)^{\mathrm{T}}\mathbf{X}^k]^{-1}(\mathbf{X}^k)^{\mathrm{T}}\mathbf{S}^k \tag{12}$$

The Levenberg–Marquardt method adopts a damping term to cope with ill-posed characteristics such that

$$\mathbf{P}^{k+1} = \mathbf{P}^k - [(\mathbf{X}^k)^{\mathrm{T}}\mathbf{X}^k + \mu^k\boldsymbol{\Omega}^k]^{-1}(\mathbf{X}^k)^{\mathrm{T}}\mathbf{S}^k \tag{13}$$

where μ is a positive scalar named damping parameter, and $\boldsymbol{\Omega}^k = \mathrm{diag}[(\mathbf{X}^k)^{\mathrm{T}}\mathbf{X}^k]$ is a diagonal matrix [4].

2.5. Automatic differentiation (AD)

No matter how complicated the objective function, it is executed on computer as a sequence of code events containing only elementary operations such as addition, subtraction, multiplication or division. By applying chain rule on every code event, the sensitivity coefficients can be calculated. Based on this fact, a program code for the calculation of sensitivity coefficients can be directly extracted from the code of direct problem. For this reason, this method does not need to derive an adjoint problem or a sensitivity problem so that their discretization procedure for solving those problems is not necessary either.

Rather, it needs following two steps for automatic differentiation. Firstly, the objective function for differentiation should be broken into its most elementary forms. Each elementary form permits only one computational operation such as addition, subtraction, multiplication or division. Secondly, the code event is sequentially differentiated in the form of total derivatives.

There are two approaches to calculate sensitivity matrix in AD, i.e. source transformation and operator overloading. The former is to change the source code following the previously described manner such that the source code is decomposed into elementary code events. The latter does not decompose the source code, but instead uses a derived type of modern compiler. It needs a modern compiler to overload elemental operator such as intrinsic functions in the FORTRAN. Since the variables for differentiation have a derived type comprised of the function value, the first and the second order derivatives, the redefinition of operators is needed. In this approach, all we have to do is just to define all variables involved in the calculation of differentiation in derived type. This requires, however, more additional computational resource since all variables involved in the calculation of differentiation should be defined in derived type. We adopted ADIFOR as source transformation type in this work [10].

There are two modes, i.e. forward and backward, according to the direction applying chain rule to code event. In this study, the forward mode is adopted, while its general formulation of differentiation by chain rule in forward mode is written by

$$\frac{\partial S_i}{\partial e_j} = \sum_{k=n_p+1}^{n_c} \frac{\partial S_i}{\partial e_k}\frac{\partial e_k}{\partial e_j}, \quad i = 1, \ldots, n_{\mathrm{e}} \quad \text{and} \quad j = 1, \ldots, n_{\mathrm{p}} \tag{14}$$

where n_{c} is the number of code events.

2.6. Broyden combined update (BC)

The various secant methods have been studied by many researchers for their convenience in calculating the gradient value [13–15]. They utilize the function values of present and previous iterations to obtain the gradient information. Broyden's method for nonlinear systems belongs to the present type. The Levenberg–Marquardt method (LMM) finds the solution with following iteration procedure:

$$\mathbf{P}^{k+1} = \mathbf{P}^k + \boldsymbol{\Delta}_k \tag{15}$$

$$\boldsymbol{\Delta}_k = -[(\mathbf{X}^k)^{\mathrm{T}}\mathbf{X}^k + \mu^k\boldsymbol{\Omega}^k]^{-1}(\mathbf{X}^k)^{\mathrm{T}}\mathbf{S}^k \tag{16}$$

The Broyden's method approximates $\mathbf{X}^k$ by $\mathbf{B}_k$ so that it does not involve any computing derivative at all. Moreover, $\mathbf{B}_{k+1}$ is obtained from $\mathbf{B}_k$ using simple procedures, so called, update.

Broyden's good method (BGM) is defined by

$$\mathbf{B}_{k+1} = \mathbf{B}_k + \frac{(\mathbf{y}_k - \mathbf{B}_k\boldsymbol{\Delta}_k)\boldsymbol{\Delta}_k^{\mathrm{T}}}{\boldsymbol{\Delta}_k^{\mathrm{T}}\boldsymbol{\Delta}_k} \tag{17}$$

Here, $\mathbf{y}_k = \mathbf{S}(\mathbf{P}_{k+1}) - \mathbf{S}(\mathbf{P}_k)$ is the difference in function values of previous and present iteration. Additionally, the definition of Broyden's bad method (BBM) is

$$\mathbf{B}_{k+1} = \mathbf{B}_k + \frac{(\mathbf{y}_k - \mathbf{B}_k\boldsymbol{\Delta}_k)\mathbf{y}_k^{\mathrm{T}}\mathbf{B}_k}{\mathbf{y}_k^{\mathrm{T}}\mathbf{B}_k\boldsymbol{\Delta}_k} \tag{18}$$

The name of method does not indicate that BGM is superior to BBM. In [13], a combined method was devised to choose BGM or BBM according to the test rule as defined by

$$\frac{|\boldsymbol{\Delta}_k^{\mathrm{T}}\boldsymbol{\Delta}_{k-1}|}{|\boldsymbol{\Delta}_k^{\mathrm{T}}(\mathbf{X}_k)^{-1}\mathbf{y}_k|} < \frac{|\mathbf{y}_k^{\mathrm{T}}\mathbf{y}_{k-1}|}{\mathbf{y}_k^{\mathrm{T}}\mathbf{y}_k} \tag{19}$$

If the above condition is satisfied, BGM is applied, otherwise, BBM is selected.

The Broyden combined update turned out to be superior to BGM or BBM alone. In order to use this method, the first Jacobian value, $\mathbf{B}_0$, should be provided using finite-difference approximation (FD) or AD.

2.7. Inverse analysis procedure

In order to estimate the total heat flux distribution on heater surface satisfying the desired total heat flux and temperature on design surface, all properties are assumed to be known except the total heat flux distribution on heater surface. The computational algorithm for inverse problem can be summarized as follows. Suppose that desired total heat flux $\mathbf{q}^*_{T,d} = (q^*_{T,d,1}, q^*_{T,d,2}, \ldots, q^*_{T,d,n_e})$ and temperature are given at each element on design surface and an initial guess $\mathbf{P}^0$ is available. The solution is sought by the following iterative steps:

1. Knowing $\mathbf{P}^k$, compute $I^*(\vec{r}, \hat{s})$ in Eq. (2) by solving the direct problem with boundary condition of Eq. (3), and calculate non-dimensional incident radiation, G^* and radiative heat flux of Eq. (4) on design surface, $\mathbf{q}^*_{R,d}$.
2. Knowing G^*, compute internal temperature distribution Θ from Eq. (1), and calculate non-dimensional conductive heat flux on design surface, $\mathbf{q}^*_{C,d}$, given by Eq. (5).
3. Calculate non-dimensional total heat flux on design surface, $\mathbf{q}^*_{T,d}$, given by Eq. (6).
4. Check the stopping criterion. If $\max\left(\frac{\mathbf{P}^{k+1}-\mathbf{P}^k}{\mathbf{P}^{k+1}}\right) \leqslant 10^{-6}$, all calculation steps are terminated, otherwise, the inverse procedure is continued.
5. Compute the sensitivity matrix $\mathbf{X}$ with methods of AD from Eq. (14) or BC from Eqs. (17)–(19).
6. Knowing Ω^k, compute $\mathbf{P}^{k+1}$ from Eq. (13). Replace $k+1$ by k and return to step 1.

3. Results and discussion

3.1. Validation of FVM code for combined radiation and conduction

FVM code was applied for validation to infinite concentric cylinders with isothermal diffuse boundaries, since results obtained by exact formulation [1] and discrete ordinates method (DOM) [3] are available in the literatures. In order to simulate infinite concentric cylinders, cyclic condition was imposed on east and west boundary, that is, outward intensity in east boundary was set as inward intensity in west boundary if solid angle is the same, and vice versa, respectively. Additionally, the ratio of outer radius to cylinder length was set to 1/10. Non-dimensional temperature distribution, $\frac{\Theta(r)-\Theta(r_{\mathrm{out}})}{\Theta(r_{\mathrm{in}})-\Theta(r_{\mathrm{out}})}$, for various scattering albedo was computed for comparison with other results under the condition of $\beta r_{\mathrm{in}} = 1, \beta r_{\mathrm{out}} = 2$, $\Theta(r_{\mathrm{in}}) = 1$, $\Theta(r_{\mathrm{out}}) = 0.1$, $\varepsilon(r_{\mathrm{in}}) = \varepsilon\,(r_{\mathrm{out}}) = 0.5$, $N_{\mathrm{CR}} = 0.03$.

Fig. 3 shows the results acquired by various methods of Monte-Carlo, DOM and the present FVM. The results are in good agreement one another. Based on this comparison, the computational code developed is considered as validated for next analysis.

3.2. Inverse problem

First of all, in order to simulate a desired total heat flux, a direct problem was solved using Eqs. (1)–(6) given boundary conditions and medium properties as depicted in Fig. 1b. After obtaining the simulated desired total heat flux, we inversely tried to estimate an appropriate boundary temperature on heater surface to figure out that the inverse method proposed here works properly.

Fig. 4 shows the estimated boundary temperature on heater surface and resulting total heat flux on heater and design surface. The boundary temperature distribution on heater surface was very accurately estimated. In this study, the downward direction is defined as positive for total heat flux on design and heater surfaces.

Comparison of computational time required for calculating sensitivity matrix was carried out to investigate the efficiency of AD and BC. Finite-difference approximation

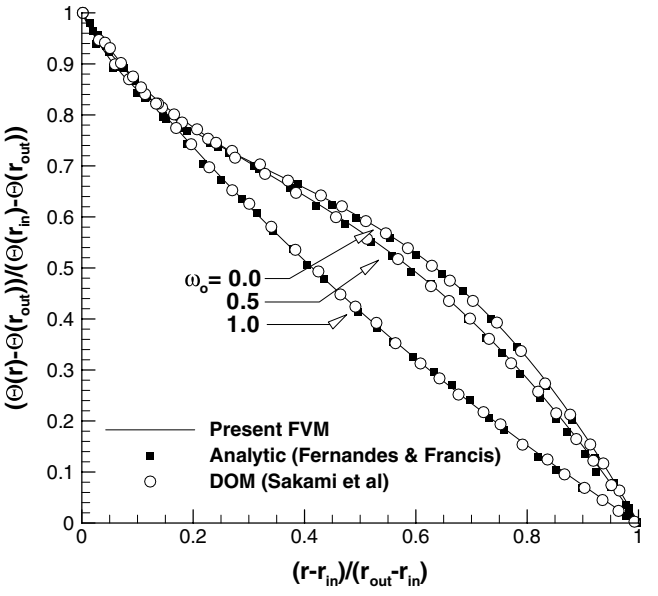

Fig. 3. Dimensionless temperature distribution for various scattering albedos.

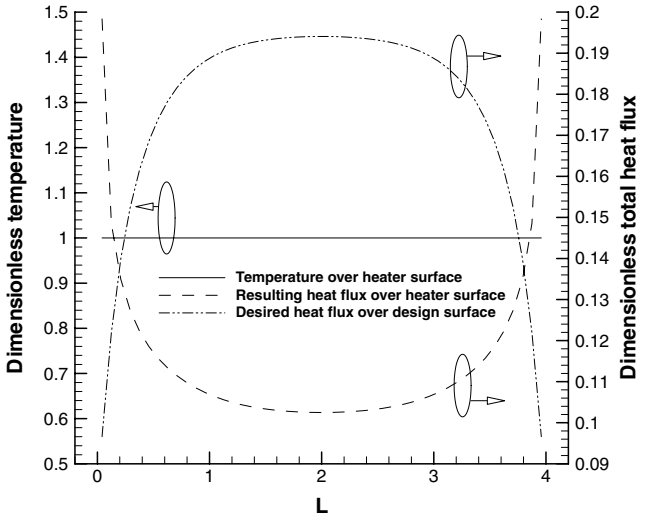

Fig. 4. Estimated temperature on heater surface and resulting total heat flux on heater and design surfaces ($N_{CR} = 0.01$, $\beta_0 = 1$, $\omega_0 = 0.5$, $r_{out} = 1$, $r_{in} = 0.5$, $L = 4$, $\theta_1 = \theta_3 = \theta_4 = 0.5$, $\varepsilon_1 = 1.0$, $\varepsilon_2 = \varepsilon_3 = \varepsilon_4 = 0.8$).

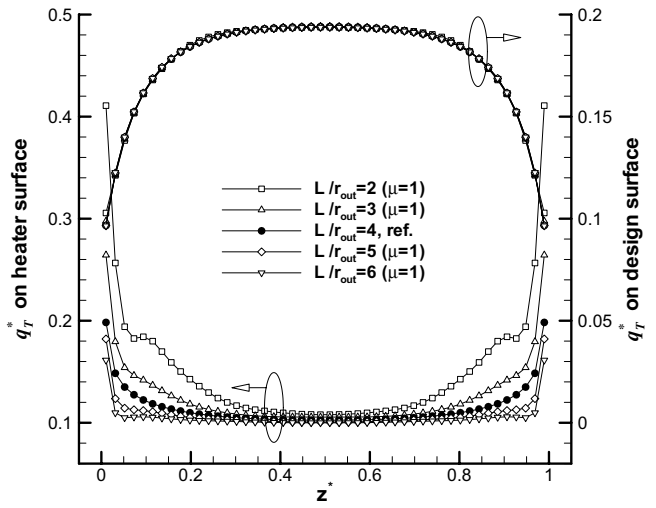

Fig. 5. Estimated total heat flux distributions on heater surface satisfying desired condition for various ratios of cylinder length to outer radius and resulting total heat flux on design surface at $k = 5$ ($N_{CR} = 0.01$, $\beta_0 = 1$, $\omega_0 = 0.5$, $r_{out} = 1$, $r_{in} = 0.5$, $\theta_1 = \theta_3 = \theta_4 = 0.5$, $\varepsilon_1 = 1.0$, $\varepsilon_2 = \varepsilon_3 = \varepsilon_4 = 0.8$).

with forward approximation was adopted as reference as follows ($\varepsilon = 10^{-6}$ is used).

$$\frac{\partial S_i}{\partial P_j} = \frac{\partial q^*_{T,e,i}}{\partial P_j} \cong \frac{q^*_{T,e,i}(P_1,\ldots,P_j+\varepsilon P_j,\ldots,P_{n_p}) - q^*_{T,e,i}(P_1,\ldots,P_j,\ldots,P_{n_p})}{\varepsilon P_j} \quad \text{for } i = 1,\ldots,n_e \quad \text{and} \quad j = 1,\ldots,n_p. \tag{20}$$

Maximum optimization level was used in FORTRAN compiler, when using Pentium IV 3.0 GHz processor. When BC was used with the Levenberg–Marquardt method (LMM), more iteration number was needed than AD and FD as shown in Table 1, since BC uses an average rate of change instead of an instantaneous rate of change. However, BC was observed to expend the shortest computational time. The result shows that BC is efficient as well as accurate enough to estimate unknown parameters so that we adopted BC as sensitivity methods for inverse analysis given below, while AD is used for $\mathbf{B}_0$.

3.3. Effect of ratio of cylinder length to outer radius

The effect of a ratio of cylinder length to outer radius on the total heat flux distribution was considered at various dimensionless positions defined as $z^* = z/L$ on the heater surface. When the ratio was changed from the reference value, $L/r_{out} = 4$, some damping was necessary to obtain a smooth and stable solution. For this reason, $\mu = 1$ was used. Fig. 5 shows the total heat flux distributions on heater and design surface for the various ratios of cylinder length to outer radius, when the desired total heat flux on design surface for $L/r_{out} = 4$ is satisfied. As the ratio increases, the total heat flux distribution on heater surface becomes more uniform. This result indicates that the desired total heat flux on design surface can be achieved with heater with more uniform heat flux as the length of heater surface is extended.

3.4. Effect of emissivity of side walls

When the emissivity of side walls of 3 and 4 is changed, the variation of total heat flux on heater surface, which satisfies the minimization of the difference in estimated and desired heat fluxes on design surface, is shown in Fig. 6. The result shows that the magnitude of total heat flux on heater surface near the side walls becomes bigger than that for reference value, $\varepsilon_{3,4} = 0.8$, when the wall emissivity increases but the desired total heat flux for $\varepsilon_{3,4} = 0.8$ is satisfied. This is because the wall with higher emissivity absorbs more heat. Even though the emissivity was significantly changed, the corresponding inverse solution satisfying its relevant desired heat flux was successfully found.

3.5. Effect of temperature at side walls

When temperature at side walls of 3 and 4 increases, the magnitude of total heat flux on heater surface near the side walls becomes smaller than that for reference value,

Table 1
Comparison of iteration number and computational time for three cases of LMM + FD, LMM + AD, and LMM + BC

Initial value	LMM + FD		LMM + AD		LMM + BC (AD used for $\mathbf{B}_0$)	
	Iteration No.	CPU time (s)	Iteration No.	CPU time (s)	Iteration No.	CPU time (s)
0.8	6	5746.78	6	3380.53	12	1019.10

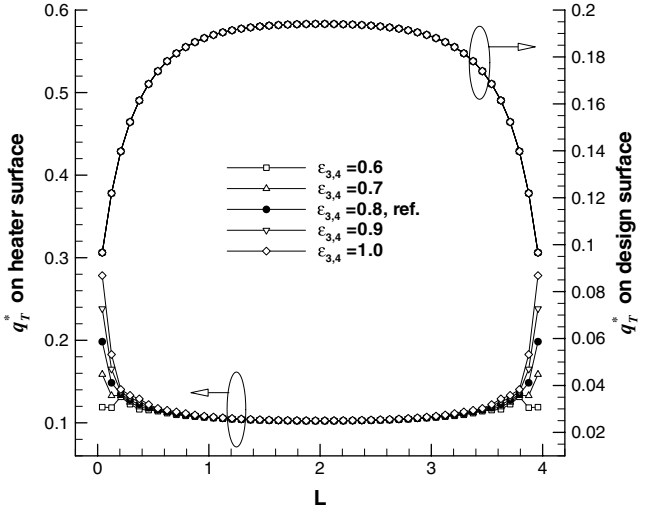

Fig. 6. Estimated total heat flux distributions on heater surface satisfying desired condition for various wall emissivities and resulting total heat flux on design surface ($N_{CR} = 0.01$, $\beta_0 = 1$, $\omega_0 = 0.5$, $r_{out} = 1$, $r_{in} = 0.5$, $L = 4$, $\theta_1 = \theta_3 = \theta_4 = 0.5$, $\varepsilon_1 = 1.0$, $\varepsilon_2 = 0.8$).

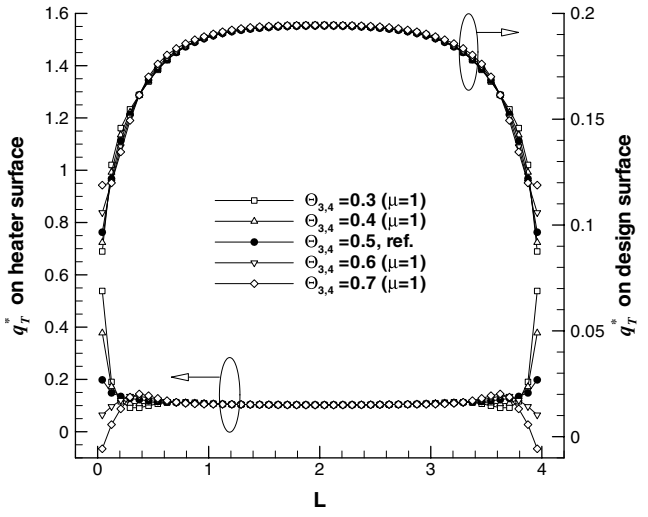

Fig. 7. Estimated total heat flux distributions on heater surface satisfying desired condition for various side wall temperatures and resulting total heat flux on design surface at $k = 5$ ($N_{CR} = 0.01$, $\beta_0 = 1$, $\omega_0 = 0.5$, $r_{out} = 1$, $r_{in} = 0.5$, $L = 4$, $\theta_1 = 0.5$, $\varepsilon_1 = 1.0$, $\varepsilon_2 = \varepsilon_3 = \varepsilon_4 = 0.8$).

$\Theta_{3,4} = 0.5$ as shown in Fig. 7. This is because more heat is supplied from the side walls when the desired total heat flux for $\Theta_{3,4} = 0.5$ is satisfied. This effect is more significant than that of wall emissivity, since the effect of wall emissivity is indirect compared with the wall temperature effect. In seeking the effects of side wall temperature, a damping is needed to obtain the stable inverse solution at $k = 5$.

3.6. Effect of conduction-to-radiation parameter

As the magnitude of conduction-to-radiation parameter becomes larger, the amplitude of oscillation becomes larger as shown in Fig. 8. This is due to the fact that the sensitivity

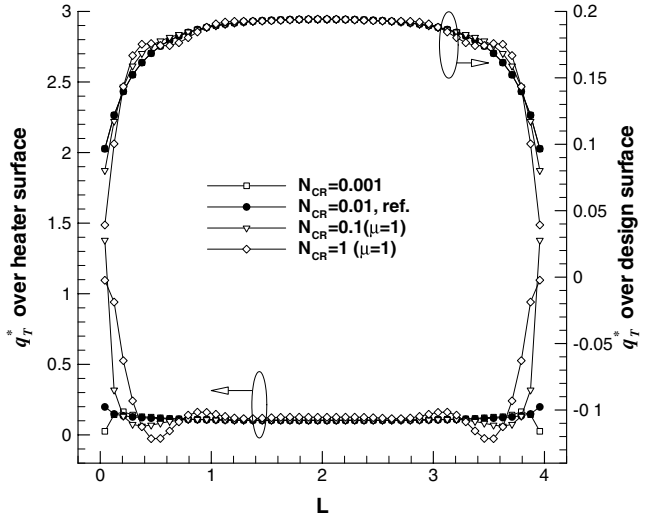

Fig. 8. Estimated total heat flux distributions on heater surface satisfying desired condition for various conduction-to-radiation parameter and resulting total heat flux on design surface ($\beta_0 = 1$, $\omega_0 = 0.5$, $r_{out} = 1$, $r_{in} = 0.5$, $L = 4$, $\theta_1 = \theta_3 = \theta_4 = 0.5$, $\varepsilon_1 = 1.0$, $\varepsilon_2 = \varepsilon_3 = \varepsilon_4 = 0.8$).

value becomes smaller when the conduction heat transfer becomes more dominant than radiative heat transfer. For this reason, the estimation of total heat flux near the boundary becomes more difficult by using the gradient-based method. In cases of $N_{CR} = 0.1$ and 1, a damping was needed to get smooth solution. Even though the damping parameter was applied, a minus heat flux was predicted for the case of $N_{CR} = 1$. In such a case, the stochastic method such as genetic algorithm would yield a better estimation solution.

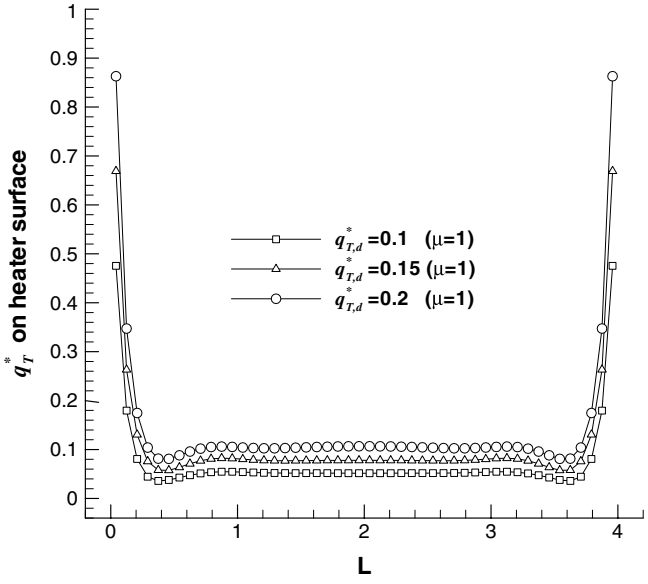

Fig. 9. Estimated total heat flux distributions on heater surface satisfying various desired conditions on design surface at $k = 5$ ($N_{CR} = 0.01$, $\beta_0 = 1$, $\omega_0 = 0.5$, $r_{out} = 1$, $r_{in} = 0.5$, $L = 4$, $\theta_1 = \theta_3 = \theta_4 = 0.5$, $\varepsilon_1 = 1.0$, $\varepsilon_2 = \varepsilon_3 = \varepsilon_4 = 0.8$).

3.7. Example as a real design problem

The methodology used in this study was applied to deal with a real design problem in which its inverse solution is not a priori known. On design surface, two boundary conditions of uniform dimensionless temperature, $\Theta_1 = 0.5$, and total heat fluxes, $q^*_{T,d} = 0.1, 0.15$ or 0.2 are imposed. In order to inspect its convergence more carefully, a damping parameter of $\mu = 1$ was applied. Fig. 9 shows the inverse solution satisfying each imposed condition. As the desired total heat flux increases, total heat flux on heater surface also increases to provide more heat flux on design surface. Fig. 10 shows their resulting total heat flux distributions on design surface calculated with estimated heat flux on heater surface in Fig. 9. It is observed that an almost uniform heat flux could be achieved except for both end regions. Since the previous result showed that the increment in side wall temperature induced a decrease in total heat flux at end regions of the heater surface, several side wall temperatures were tested to obtain a more uniform total heat flux distribution on heater surface for $q^*_{T,d} = 0.2$. Fig. 11 shows that the total heat flux distribution on heater surface becomes more uniform when the side wall temperature increases up to $\Theta_{3,4} = 0.8$. However, when $\Theta_{3,4}$ becomes 0.9, a minus heat flux appears at each end region. Fig. 12 shows resulting total heat flux distributions on design surface for various side wall temperatures. As it increases, the total heat flux distribution in the middle region becomes more uniform. However, an extraordinary change in total heat flux occurs at end regions because of the restriction of boundary condition.

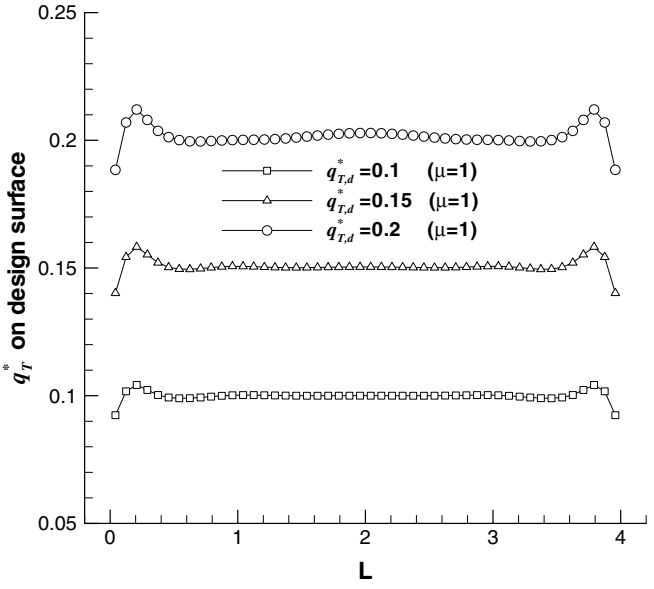

Fig. 10. Resulting total heat fluxes on design surface at $k = 5$.

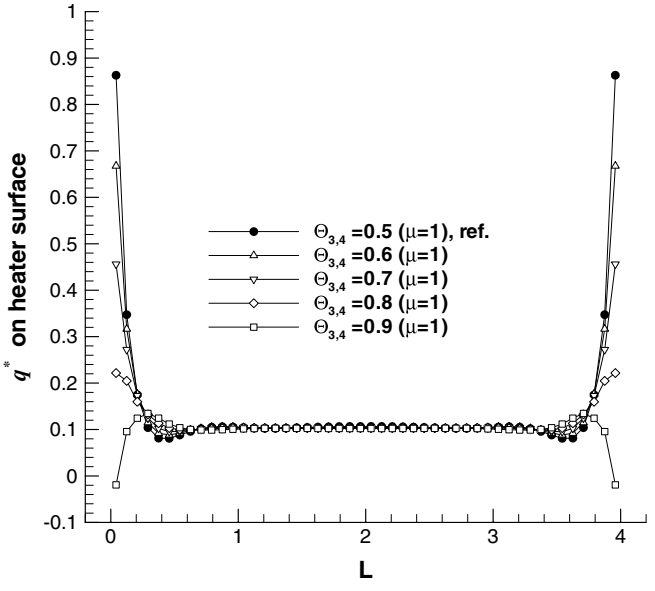

Fig. 11. Variation of total heat flux on heater surface for various side wall temperatures at $k = 5$ ($N_{CR} = 0.01$, $\beta_0 = 1$, $\omega_0 = 0.5$, $r_{out} = 1$, $r_{in} = 0.5$, $L = 4$, $\theta_1 = 0.5$, $\varepsilon_1 = 1.0$, $\varepsilon_2 = \varepsilon_3 = \varepsilon_4 = 0.8$, $q^*_{T,d} = 0.2$).

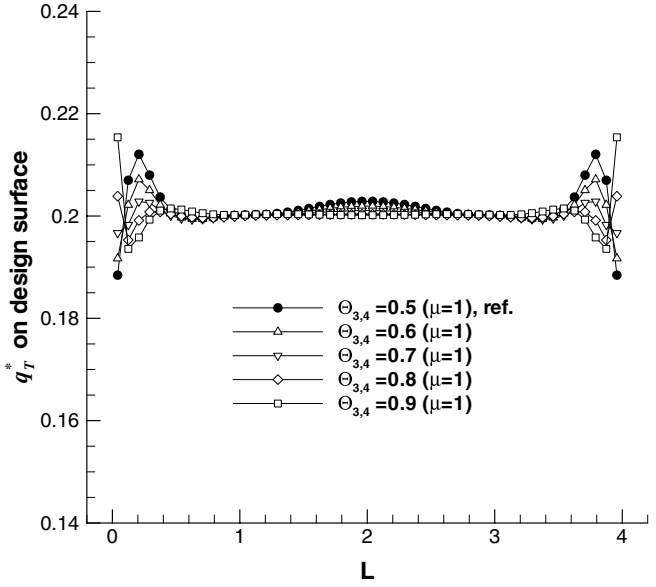

Fig. 12. Resulting total heat fluxes on design surface for various boundary temperatures at $k = 5$.

4. Conclusions

Inverse radiation–conduction design analysis in a two-dimensional concentric cylindrical absorbing, emitting and scattering medium has been conducted, given desired boundary conditions on the design surface. By adopting the automatic differentiation and the Broyden combined update as a sensitivity method, the computational time for calculating sensitivity matrix could be reduced up to 1/6 compared with that required for the finite-difference approximation.

Various parametric analyses have shown that in most cases the total heat flux on heater surface satisfying the desired condition on design surface could be well estimated using the current inverse analysis. However, it must be

noted that a stable and smooth solution could be obtained by controlling the damping parameter when the Levenberg–Marqurdt method was used for ill-posed case.

Finally, the inverse method was applied to a real design problem to get the total heat flux on heater surface satisfying uniform heat flux and temperature distribution on design surface. The desired heat flux distributions could be achieved except for both end regions. This shortcoming is considered to be successfully eliminated through the extension of heater surface length. Additionally, more uniform total heat flux distribution in the middle region on design surface and at each end region on heater surface could be obtained by increasing the side wall temperatures.

Acknowledgement

This work was supported by Grant No. R01-2006-000-11311-0 from the Basic Research Program of the Korea Science and Engineering Foundation.

References

[1] R. Fernandes, J. Francis, Combined conductive and radiative heat transfer in an absorbing, emitting, and scattering cylindrical medium, J. Heat Transfer 104 (1982) 594–601.

[2] H.Y. Li, M.N. Özisik, Simultaneous conduction and radiation in a two-dimensional participating cylinder with anisotropic scattering, J. Quant. Spectrosc. Radiat. Transf. 46 (1991) 393–404.

[3] M. Sakami, A. Charette, V. Ledez, Application of the discrete ordinate method to combined conductive and radiative heat transfer in a two-dimensional complex geometry, J. Quant. Spectrosc. Radiat. Transf. 56 (1996) 517–533.

[4] M.N. Özisik, H.R.B. Orlande, Inverse Heat Transfer, Taylor & Francis, New York, 2000 (Chapter 1).

[5] L.K. Matthews, R. Viskanta, F.P. Incropera, Development of inverse methods for determining thermophysical and radiative properties of high-temperature fibrous materials, Int. J. Heat Mass Transfer 27 (1984) 487–495.

[6] N.J. Ruperti Jr., M. Raynaud, J.F. Sacadura, A method for the solution of the coupled inverse heat conduction–radiation problem, J. Heat Transfer 118 (1996) 10–17.

[7] H.Y. Li, Estimation of thermal properties in combined conduction and radiation, Int. J. Heat Mass Transfer 42 (1999) 565–572.

[8] S.M.H. Sarvari, J.R. Howell, S.H. Mansouri, Inverse boundary design conduction–radiation problem in irregular two-dimensional domains, Numer. Heat Transfer, Part B 44 (2003) 209–224.

[9] K.W. Kim, S.W. Baek, Comparison of sensitivity methods for the function estimation of boundary conditions by inverse radiation analysis, Progress in Computational Heat and Mass Transfer, vol. 2, Lavoisier, France, 2005, pp. 1385–1390.

[10] C. Bischof, A. Carle, P. Khademi, A. Mauer, P. Hovland, ADIFOR2.0 User's guide (Revision D), Argonne National Lab. Tech. Memorandum ANL/MCS-TM-192, and CRPC Tech. Rept. CRPC-TR95516-S, USA, 1998.

[11] S.V. Patankar, Numerical Heat Transfer and Fluid Flow, Hemisphere Publishing Corporation, Washington, 1980.

[12] E.H. Chui, G.D. Raithby, P.M.J. Hughes, Prediction of radiative transfer in cylindrical enclosure with the finite volume method, J. Thermophys. Heat Transf. 6 (1992) 605–611.

[13] J.M. Martínez, Practical quasi-Newton methods for solving nonlinear systems, J. Comput. Appl. Math. 124 (2000) 97–121.

[14] J.E. Dennis, R.B. Schnabel, Numerical Methods for Unconstrained Optimization and Nonlinear Equations, Prentice-Hall, Englewood Cliffs, New Jersey, USA, 1983 (Chapter 8).

[15] K. Daun, J.R. Howell, Optimization of transient heater settings to provide spatially uniform transient heating in manufacturing processes involving radiant heating, Numer. Heat Transf., Part A 46 (2004) 651–668.